CHAPTER 8

Magnetic Actuators Operated by AC

Because alternating current (AC) voltage is commonly available, many magnetic actuators are designed for AC operation. In most cases, the direct current (DC) actuators of the preceding chapter must be substantially modified for AC operation. Armatures of clapper type and plunger type are still common, but changes to both the steel core and the coils are usually required.

8.1 SKIN DEPTH

Chapter 2 has shown that time-varying magnetic fields induce eddy currents in conducting materials. Since AC currents produce time-varying magnetic fields, eddy currents are a key issue in AC magnetic actuators. An easy way to examine AC eddy current effects is to calculate *skin depth.*

Faraday's law of Chapter 2 can be used to find the skin depth [1]:

$$\delta = \frac{1}{\sqrt{\pi f \mu \sigma}} \tag{8.1}$$

where f is the AC frequency in Hz, μ is the permeability, and σ is the electrical conductivity. Both the steel core and the coils of magnetic actuators are made of conducting materials, and thus the skin depth is often smaller than typical core or wire dimensions. Skin depth in wires will be discussed in Chapter 12, while here skin depth in steel cores is examined. For example, the 60 Hz magnetic flux in Example 6.5 was seen in Figure E6.5.1 to be concentrated near the outer skin of its cylindrical steel core. Such flux concentration on the skin, and lack of flux in the interior, is called *skin effect.* The skin depth of (8.1) is the depth at which flux density and eddy currents have decayed to $1/e$ of their surface value, or 36.8%. The decay from surface into the interior is exponential [1].

Note that skin depth of (8.1) is infinite for DC (0 frequency), but decreases inversely proportional to the square root of frequency. It is also inversely proportional to the

Magnetic Actuators and Sensors, Second Edition. John R. Brauer.
© 2014 The Institute of Electrical and Electronics Engineers, Inc. Published 2014 by John Wiley & Sons, Inc.

product of permeability times conductivity. This product is especially high for steel. Steel in magnetic actuators and sensors typically has permeabilities thousands of times that of air, and has conductivities on the order of 1.E6 S/m. In Example 6.5, the relative permeability of 2000, conductivity of 2.E6 S/m, and frequency 60 Hz in (8.1) gives a skin depth of 1 mm. Note that the flux lines in Figure E6.5.1 are indeed concentrated in the outer 1 mm or so of the 10-mm radius steel core. The inner 9-mm steel region is essentially unused for AC, and it could be removed to save weight and cost.

To carry more flux than just the skin will allow, most AC steel cores are laminated as was shown in Figure 2.6 and described in Chapter 2. The lamination thickness should be less than approximately 0.5–1 mm skin depth. Thus most steel laminations for 60 Hz AC operation are less than 1 mm thick. For example, the Eaton AC magnetic actuator of Figure 4.3 has steel of depth 28.5 mm into the page and is made of approximately 46 laminations, each approximately 0.62 mm thick. Both its stator and its armature are made of laminations that have been punched from sheet steel and then stacked and held together by rivets.

8.2 POWER LOSSES IN STEEL

8.2.1 Laminated Steel

Laminating steel does not completely eliminate steel eddy currents and their losses, but greatly reduces them. As long as the lamination thickness t is considerably less than skin depth, the eddy power loss density can be shown to obey [2] the following formula:

$$\frac{P_e}{v} = \frac{t^2\omega^2 B^2 \sigma}{24} \tag{8.2}$$

where B is the peak magnetic flux density, $\omega = 2\pi f$, P_e is power in watts, and v is the volume of the conducting material in cubic meters. The above loss equation holds true when the eddy currents cause negligible changes in the magnetic field. If the skin depth is less than the lamination thickness, more complicated relations often apply [2], and the laminations do not carry nearly as much flux.

In addition to eddy current loss, steel carrying AC flux has *hysteresis loss.* As explained in Chapter 5, areas on B–H planes correspond to energy, and hysteresis causes the B–H relation to have more than one single-valued curve. Thus in Figure 8.1, which shows typical B–H loops for AC and H, the energy density lost per cycle is the area enclosed by the B–H loop. Hysteresis loss is significant whenever eddy loss of (8.2) is small due to small lamination thickness. The sum of hysteresis loss and eddy current loss is called *core loss*.

Because the energy density lost per cycle is the area of Figure 8.1, hysteresis loss is proportional to frequency. Also, for typical steel the area of Figure 8.1 is

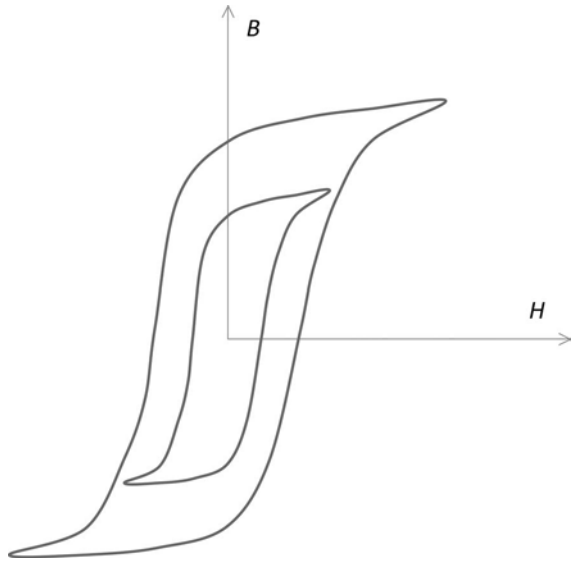

FIGURE 8.1 *B–H* hysteresis loops for AC *H* due to AC. The area enclosed is the energy lost per cycle. Two loops are shown for two different peak AC values.

approximately proportional to the peak B to the power n, where n varies from about 1.5 to about 2.5 [3]. Hence the hysteresis power loss density obeys:

$$\frac{P_h}{V} = K_h f B^n \tag{8.3}$$

where K_h is approximately constant.

Manufacturers of steel laminations for magnetic devices, often called electrical steels, customarily measure and publish *core loss curves.* Such curves are commonly available for 50 and 60 Hz over a range of peak B values.

Steel manufacturers also measure and publish *B–H* curves for AC devices called *normal AC B–H curves*. Such a normal curve is the locus of the tips of *B–H* loops such as shown in Figure 8.1. The normal AC curve may differ somewhat from the DC curve.

8.2.2 Equivalent Circuit

As discussed in Example 6.5, eddy current loss (and thus core loss) introduces a resistance in the impedance seen by the coil. Since the losses of (8.2) and (8.3) are proportional to B^2, and V_L across an inductor is proportional to B (from Faraday's law), core loss is equivalent to the parallel resistor R_{core} shown in Figure 8.2. Its power loss, like core loss, is proportional to the square of the voltage across the inductor:

$$P_{\text{core}} = V_L^2 / R_{\text{core}} \tag{8.4}$$

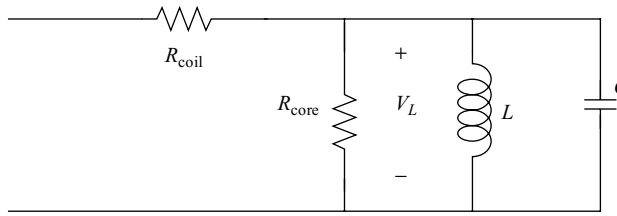

FIGURE 8.2 Equivalent circuit for a coil in a magnetic device. R_{core} accounts for core loss; R_{coil} accounts for coil loss. The nonlinear inductor accounts for flux and Faraday's law. The capacitor accounts for interwinding capacitance, which becomes important at high frequencies.

Note that Figure 8.2 also includes a capacitor due to the interwinding capacitance mentioned in Chapter 6. It also includes a series resistor R_{coil} which equals the resistance of the coil itself. As explained further in Chapter 12, if skin effects in the coil are negligible R_{coil} is the DC coil resistance, but substantial coil AC skin effects may cause R_{coil} to change somewhat.

The impedance of the capacitor is typically negligible at 60 Hz, but becomes more important the higher the frequency. Since the capacitor C and inductor L are in parallel, the coil has a natural resonant frequency:

$$f_r = \frac{1}{2\pi\sqrt{LC}} \tag{8.5}$$

As discussed in Chapter 6, finite-element software usually outputs the impedance seen by each coil. This impedance is a sum of real and imaginary parts in series:

$$Z_s = R_s + jX_s \tag{8.6}$$

and is here assumed to account only for the core loss and inductance of the coil; that is, the coil's DC resistance and capacitance are not included in (8.6). However, Figure 8.2 needs the *parallel* impedance:

$$Z_p = R_{core} + j\omega L = R_p + jX_p \tag{8.7}$$

An advantage of the parallel impedance is that when the coil is excited by a voltage V_s, the core current loss draws an extra current, the current through the parallel resistor.

To find R_p and X_p of Figure 8.2, apply the parallel circuit formula:

$$R_s + jX_s = \frac{(R_p)(jX_p)}{R_p + jX_p} \tag{8.8}$$

Using complex AC circuit methods, (8.8) can be expressed in terms of magnitudes and phase angles as:

$$R_s + jX_s = \frac{R_p X_p \angle 90^\circ}{\left(R_p^2 + X_p^2\right)^{1/2} \angle \arctan \dfrac{X_p}{R_p}} \tag{8.9}$$

$$\left(R_s^2 + X_s^2\right)^{1/2} \angle \arctan \frac{X_s}{R_s} = \frac{R_p X_p}{\left(R_p^2 + X_p^2\right)^{1/2}} \angle 90^\circ - \arctan \frac{X_p}{R_p} \tag{8.10}$$

The magnitudes on both sides must be the same and the angles on both sides must also be the same. Also, in most cases the finite-element results will find $R_s \ll X_s$. Thus from the first term of a series expansion:

$$\arctan \frac{X_s}{R_s} \cong 90^\circ - \frac{R_s}{X_s} \tag{8.11}$$

Assuming the above equality is exact, then equating the angles of (8.10) gives:

$$\frac{R_s}{X_s} = \frac{X_p}{R_p} \tag{8.12}$$

Also, if $R_s \ll X_s$, then from the magnitudes of (8.10), it is approximately true that:

$$X_p = X_s \tag{8.13}$$

Finally, (8.12) and (8.13) obtain:

$$R_p = \frac{X_p^2}{R_s} \tag{8.14}$$

A major problem with AC equivalent circuits for devices made of nonlinear *B–H* materials is that the nonlinearity often causes the voltage and/or the current to become nonsinusoidal. The greater the current and voltage, the greater the saturation, and the more the waveforms can deviate from sinusoidal. Since the inductive reactances X_p and X_s in the above equations are constants, they cannot fully represent nonlinear behavior. However, these reactances can approximately simulate saturation effects when their magnitudes decrease as current and flux rise. These effective reactances are often obtained by AC finite-element software by use of "effective permeability" which decreases with current magnitude [4].

For more exact modeling, and to obtain nonsinusoidal waveforms, nonlinear transient techniques of Chapters 9 and 14 are required. Chapter 14 will also discuss special AC magnetic actuators designed to produce reciprocating (back and forth) force and motion, while this chapter concerns AC actuators that produce force and motion in only one direction.

8.2.3 Solid Steel

The equivalent circuit of Figure 8.2 still applies if some or all of the steel is solid. However, the simple equations for the eddy current loss and hysteresis loss derived above for laminated steel no longer apply. In most cases, the eddy current loss in solid steel greatly exceeds the hysteresis loss, which can thus be neglected. The best way to predict the steel power loss and equivalent circuit parameters is to use the finite-element method.

Solid steel is sometimes used in AC actuators, depending on the type (from Chapter 7):

- *For planar actuators with clapper armatures*, the stator is easily laminated, but often the armature is made of solid steel, especially if the armature is steel plate (or steel scrap) to be lifted by a *lifting magnet*.
- *For axisymmetric actuators with clapper armatures,* lamination is difficult and expensive, and thus both stator and armature steels are usually solid.
- *For planar actuators with plunger armatures,* both stator and armature are usually laminated, but a solid armature is sometimes required due to its greater mechanical rigidity.
- *For axisymmetric actuators with clapper armatures,* lamination is difficult and expensive, and thus both stator and armature steels are usually solid.

The easiest way to design and manufacture an AC actuator is to simply apply AC to an existing DC solenoid. However, such a simple design method is usually unsatisfactory. Besides the need to laminate to reduce eddy power loss, the number of turns usually must be changed to obtain the proper current for the particular AC voltage applied. Further changes are discussed in the remainder of this chapter.

Example 8.1 AC Flux Linkage and Equivalent Circuits of Solenoid of Example 7.1 with a Solid Steel Clapper Figure E8.1.1 shows the solenoid of Example 7.1 turned upside down to act as an AC lifting magnet. The stator is laminated

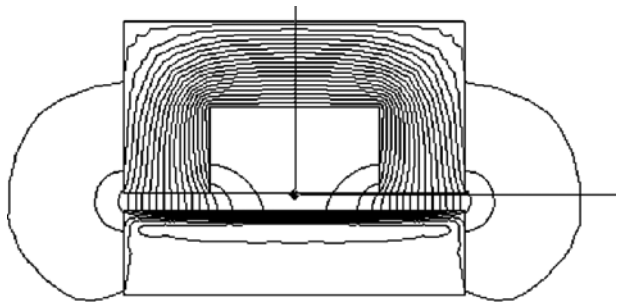

FIGURE E8.1.1 Computer display of AC magnetic actuator with a laminated steel stator and solid steel rotor. Its dimensions are the same as those in Figure E7.1.1. The flux lines are computed for a frequency of 60 Hz.

but the clapper being lifted is solid steel. The stator winding shown has 200 turns carrying 2-A rms AC 60-Hz current. The dimensions are $w = 10$ mm, $Al_1 = 5$ mm, $Al_2 = 30$ mm, $Al_3 = 5$ mm, $Sl_1 = 15$ mm, $Sl_2 = 30$ mm, $Sl_3 = 15$ mm, $g = 2$ mm. Assuming all steel has relative permeability of 2000, and the clapper has conductivity 2.E6 S/m, find the AC fields and series and parallel equivalent circuits using Maxwell 2D planar finite-element software. Assume that the stator has a depth into the page of 1 m in the z direction and that the clapper extends beyond the stator both in the $+z$ and $-z$ directions to allow end region eddy currents to flow with zero end region resistance and zero end region inductance.

Solution The flux linkage output by Maxwell is $\lambda = 1.814\text{E–}5\text{–}j7.51\text{E–}7$ per turn. The series impedance for one turn is then found using (6.31):

$$Z = j\omega\lambda/I \tag{E8.1.1}$$

where $I = 2$ A and $\omega = 377$. The resulting series impedance (for 200 turns) is:

$$Z_s = R_s + jX_s = (200)(141.6\text{E–}6 + j3.42\text{E–}3) = 28.32\text{E–}3 + j684\text{E–}3 \tag{E8.1.2}$$

Note that as expected, the resistive part is much smaller than the reactive part.

To obtain the parallel equivalent circuit of Figure 8.2, recall that $X_p = X_s$, so $X_p = 684\text{E–}3$ and $L_p = 684\text{E–}3/377 = 1.814\text{E–}3$ H. Also, use (8.14) to obtain the parallel core loss resistor:

$$R_p = \frac{X_p^2}{R_s} = 16.52\,\Omega \tag{E8.1.3}$$

Note that the parallel core loss resistor has much higher impedance than the parallel inductive reactor, as expected.

The computed flux lines are shown in Figure E8.1.1. Note the substantial skin effects in the solid steel armature. As mentioned in the problem definition, end region effects are ignored in this 2D model; adding end region effects to a 2D model will be discussed in Chapter 14. Also in that chapter, an example transformer will demonstrate the use of parallel impedances.

8.3 FORCE PULSATIONS

8.3.1 Force with Single AC Coil

Because AC actuators have AC that varies with time, Ampere's law shows that their magnetic fields B also vary with time. Since magnetic reluctance force of Chapter 5

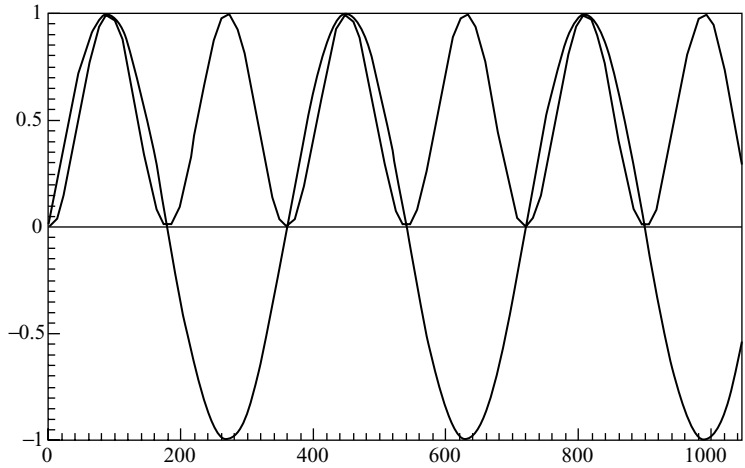

FIGURE 8.3 Current and force waveforms versus time for a single AC in an actuator. The current swings positive and negative, while the force is always positive and has double frequency content.

is approximately proportional to the square of B, the time-varying B causes force variations called *pulsations*.

If eddy currents are small enough to not affect the field, then the magnetic field throughout the actuator is due solely to the current through the energized coil or coils. Often there is only one coil, and thus there is only one AC and all fields are in phase with the current. Since the current goes through zero twice per cycle, the magnetic fields throughout the actuator must go through zero twice per cycle.

For example, the current is often a sine wave:

$$I_1 = \sin(2\pi ft) \tag{8.15}$$

Figure 8.3 plots this AC sine wave over a few cycles, when the argument of the sine is varied from 0° to about 1000°. From (5.11), the force is then proportional to:

$$F_1 = kI_1^2 = k\sin^2(2\pi ft) = \frac{k}{2}(1 - \cos 4\pi ft) \tag{8.16}$$

The force versus time waveform is also plotted in Figure 8.3. Note that the force pulsates from its maximum to zero, going through zero twice per cycle of current. The alternating component of the force has twice the electrical frequency. The average force value is one-half the maximum force, and the total force never reverses direction.

The above current and force relations assume that the current is sinusoidal, as often assumed for the reactances of Figure 8.2. In actuality, most AC solenoids are voltage driven, typically by 120 V 60 Hz in the United States. If saturation occurs, then the current may be nonsinusoidal, as mentioned in Subsection 8.2.2. However, in all cases the current goes through zero twice per cycle, and so will the force.

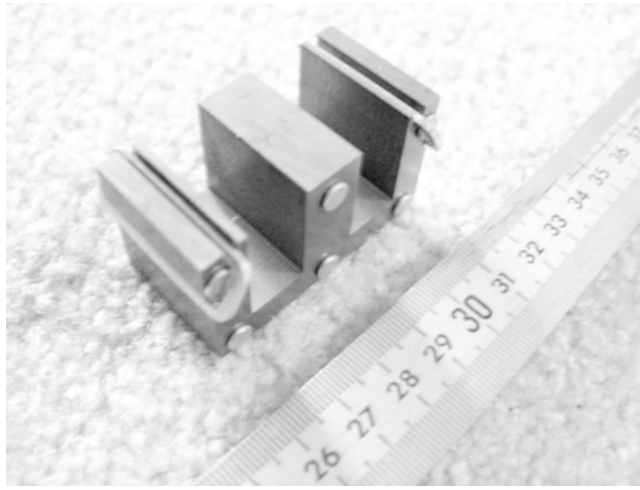

FIGURE 8.4 Photo of stator core with two shading rings in Eaton AC actuator of Chapter 4.

8.3.2 Force with Added Shading Coil

If an additional significant current at a different phase angle exists in the AC solenoid, then it is possible that the force pulsations may be reduced. For example, suppose that one winding has the current of (8.15) and produces the force of (8.16) on its steel pole, but that there is also an additional current:

$$I_2 = \cos(2\pi ft) \tag{8.17}$$

Suppose also that this current produces an additional force on its own steel pole, giving a total force:

$$F_1 + F_2 = k\left(I_1^2 + I_2^2\right) = k[\sin^2(2\pi ft) + \cos^2(2\pi ft)] = k \tag{8.18}$$

Note that a trigonometric identity has been used to obtain a magnetic force that is independent of time. Thus the force has no pulsations.

In practice, it is extremely difficult to obtain the constant force of (8.18). However, it is possible to raise the minimum force considerably above zero by a relatively inexpensive modification.

The inexpensive way of reducing the pulsation is to add a *shading coil* or a one-turn version called a *shading ring*. Figure 8.4 shows the aluminum shading rings added to the two poles in the Eaton AC actuator of Chapter 4. According to the time derivative in Faraday's law, the induced voltage in each ring will be 90° out of phase from the magnetic flux passing through it. If the induced current were in phase with that induced voltage, then the phase relation of (8.18) would be satisfied. However, due to self-inductance, the current phase lags further behind. Also, the magnitude of the induced shading ampere-turns will always be less than the magnitude of the

ampere-turns in the main coil. Thus a shading coil will not eliminate force pulsations but can reduce them.

While reluctance techniques have been used to calculate shading coil effects [5], the easiest way to calculate them is using finite-element analysis. The effects of the shading coil in the Eaton AC actuator of Figure 8.4 have been calculated using nonlinear transient finite-element analysis, including the effects of armature motion, and will be discussed in Chapter 14. Chapter 14 will also discuss AC actuators where force pulsations (actually force reversals) are desirable to create reciprocating motion.

Since induced currents in solid metals affect the force, armatures made of nonlaminated, high conductivity metal experience large eddy current forces which in some cases can be shown to be *repulsive* instead of attractive. Pure aluminum armatures placed above a steel stator with an AC stator coil can in some cases be *levitated* above the stator. That is, the magnetic repulsive force vertically upward balances the downward force of gravity [6, 7], and can be used to levitate trains.

Example 8.2 Fluxes and Forces on Axisymmetric Plunger Armature Solenoid of Example 7.4 with Added Shading Ring Figure E8.2.1 shows the axisymmetric solenoid with a plunger armature of Example 7.4 with an added shading ring on its stator pole. The number of turns of the main driven coil remain $N = 400$. The current I is now 4-A rms at 60 Hz. The dimensions remain the same as in Example 7.4, except

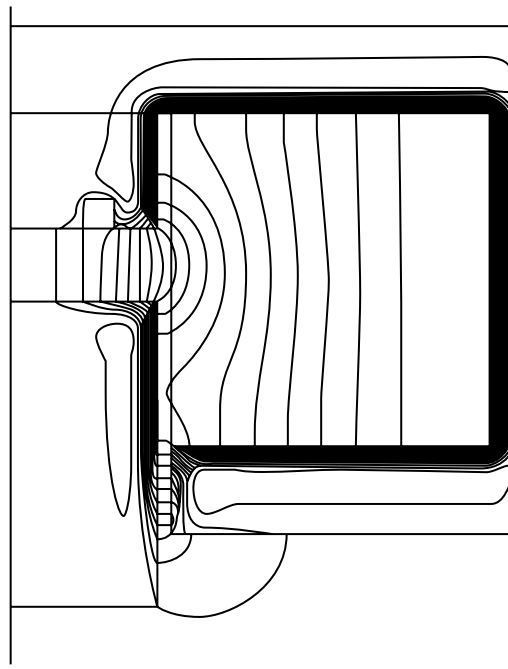

FIGURE E8.2.1 Computer display of geometry and computed flux lines of axisymmetric actuator with shading coil placed on stator pole face.

that now there is an added shading ring. The steel has relative permeability 2000 and conductivity 5.E5 S/m. The ring has an inner radius of 10 mm and a cross section of 4 mm by 4 mm. It is made of copper with conductivity 5.8E7 S/m.

Compute the magnetic fields and the force using the finite-element software Maxwell.

Solution If Maxwell SV is used, the easiest way to make this model is to modify the model of Example 7.4. The solution type must be changed to "Eddy Current." The shading ring must be added using a rectangular box command. Be sure to change the steel conductivity to the specified nonzero value, and choose copper for the shading ring material. Also be sure to specify "Force" under "Setup Executive Parameters." To allow convergence to small energy error, allow 16 passes under "Setup Solution."

If Maxwell version 16 is used, it is easiest to modify the model of Example 7.4. The solution type must be changed to "Eddy Current." The shading ring must be added using a create box command. Be sure the change the steel conductivity to the specified nonzero value, and choose copper for the shading ring material. Also be sure to assign a "Force" under "Parameters." To allow convergence to a small energy error, allow 16 passes under "Solve Setup" dialog box.

The solution has the magnetic flux line plot shown in Figure E8.2.1 at time equal to 0° phase angle. Note that skin effects are clearly visible. The force output by Maxwell has a time-average value of 8.46 N and an "AC fluctuation" of 8.40 N. Thus the fluctuation or pulsation is large, but somewhat less than the average value. Hence the shading ring prevents the force from going through zero twice per cycle.

8.4 CUTS IN STEEL

A way to improve the performance of AC magnetic devices made of solid steel is to put cuts in the steel. The cuts or slots partly block the eddy current circulation pattern, somewhat like laminations, and thereby reduce power loss and increase flux.

8.4.1 Special Finite-Element Formulation

To compute the magnetic fields and flux in slotted steel with eddy currents, an unusual finite-element formulation called "Eddy Axial" is available in Maxwell 2D (versions 12 or earlier including SV) or by using a full 3D model. Displacement currents are neglected because the frequency applied to actuators is usually 1 kHz or lower.

The formulation begins with Ampere's law with $\mathbf{J} = \sigma\mathbf{E}$ from Chapter 2:

$$\nabla \times \mathbf{H} = \sigma\mathbf{E} \tag{8.19}$$

Premultiplying both sides by the inverse of the conductivity and then taking the curl of both sides:

$$\nabla \times \sigma^{-1}\nabla \times \mathbf{H} = \nabla \times \mathbf{E} \tag{8.20}$$

Applying Faraday's law gives:

$$\nabla \times \sigma^{-1} \nabla \times \mathbf{H} = -\frac{\partial \mathbf{B}}{\partial t} \tag{8.21}$$

which for sinusoidal fields of angular frequency $\omega = 2\pi f$ is:

$$\nabla \times \sigma^{-1} \nabla \times \mathbf{H} = -j\omega\mu\mathbf{H} \tag{8.22}$$

where permeability μ is assumed constant, that is, the *B–H* curve is assumed to be operating in its linear region.

In comparison, the planar eddy current solution of Example 8.1 solves (8.19) by using $H = B/\mu$, obtaining:

$$\nabla \times \mu^{-1} \mathbf{B} = \sigma \mathbf{E} \tag{8.23}$$

Substituting (2.45) and (2.47), and again assuming sinusoidal fields gives:

$$\nabla \times \mu^{-1} \nabla \times \mathbf{A} = -j\omega\sigma\mathbf{A} \tag{8.24}$$

which is the differential equation for "Eddy Current" problems such as Example 8.1. In the 2D case, the only component of $\mathbf{A}$ is commonly the z component normal to the plane of the problem as described in Chapter 4.

The Eddy Axial solver uses planar 2D finite elements (of default depth 1 m) in which only one component of $\mathbf{H}$ exists, the component H_z perpendicular to the elements (out of the page). Computing only one unknown H_z at each finite-element node is much more computationally efficient than computing two components of $\mathbf{A}$ (A_x and A_y) for planar eddy currents, as much as $3^2 = 9$ times less expensive. After H_z is computed, the software also computes the eddy current density $\mathbf{J}$ using Ampere's law to give:

$$\mathbf{J} = \nabla \times \mathbf{H} \tag{8.25}$$

In the 2D case with $\mathbf{H} = H_z\,\mathbf{u_z}$, $\mathbf{J}$ has only x and y components in the plane of the triangular finite elements. Contours of constant H_z correspond to eddy current flow lines.

8.4.2 Loss and Reluctance Computations

The finite-element method of the preceding subsection can be used to analyze a 2D circular model of a cylindrical solid steel pole. While other steel shapes can also be analyzed, the cylinder is selected here because of its common use in axisymmetric

magnetic actuators and sensors. Also, because equations have been derived for conductors that are perfect circles without cuts, some finite-element computations can be verified by comparing them with the equations.

Equations for the AC fields in circular conductors have been derived by Ramo et al. [8] as follows. Applying vector identities to (8.22) gives:

$$\nabla^2 \mathbf{H} = j\omega\mu\sigma \mathbf{H} \tag{8.26}$$

For $\mathbf{H} = H_z\, \mathbf{u_z}$ as discussed in the preceding subsection, (8.26) can be written in cylindrical coordinates as [8]:

$$\frac{d^2 H_z}{dr^2} + \frac{1}{r}\frac{dH_z}{dr} - j\omega\mu\sigma H_z = 0 \tag{8.27}$$

where r is the radius, the only coordinate over which H varies.

The solution of (8.27) can be shown [8] to involve Bessel functions. Since (8.27) is a complex equation, Bessel functions of complex numbers are required. It is common to define [8] Bessel real and Bessel imaginary functions:

$$\text{Ber}(v) = \text{Re}[J_o j^{-1/2} v], \quad \text{Bei}(v) = \text{Im}[J_o j^{-1/2} v] \tag{8.28}$$

Using the Ber and Bei definitions, the solution of (8.27) can be shown to be [8]:

$$H_z = H_a[(\text{Ber}(2^{1/2} r/\delta) + j\text{Bei}(2^{1/2} r/\delta))/(\text{Ber}(2^{1/2} r_o/\delta) + j\text{Bei}(2^{1/2} r_o/\delta))] \tag{8.29}$$

where r_o is the outer radius is at which H_a is applied by a coil, and δ is the skin depth.

To compare the results of (8.29) with those of the finite elements of (8.22), a steel cylinder of radius 2.5 mm is selected as shown in Figure 8.5. The steel is assumed to have relative permeability 2000 and electrical conductivity 2.E6 S/m. The H_z applied to the outside of the model of Figure 8.5 is 398.1 A/m at 60 Hz, which corresponds to 1 T flux density just inside the outer radius of the steel cylinder. The computed flux lines are also shown in Figure 8.5 at the instant that the applied 398.1 A/m is peaking.

The computed flux lines in Figure 8.5 are nonuniform, due to the eddy currents in the steel. To compare the computed field distribution with the theory of (8.29), the ratio of the magnitude of H over the applied $H = 398.1$ A/m is plotted in Figure 8.6. Also plotted is the theoretical magnitude of H from (8.29), using Ber and Bei function values interpolated from tables [9]. In all cases the computed value is within 0–1% higher than the theoretical value obtained using (8.29).

As an additional verification of the finite-element formulation, the conductivity of the steel cylinder of Figure 8.5 is changed to zero. The computed flux is 19.65 μWb,

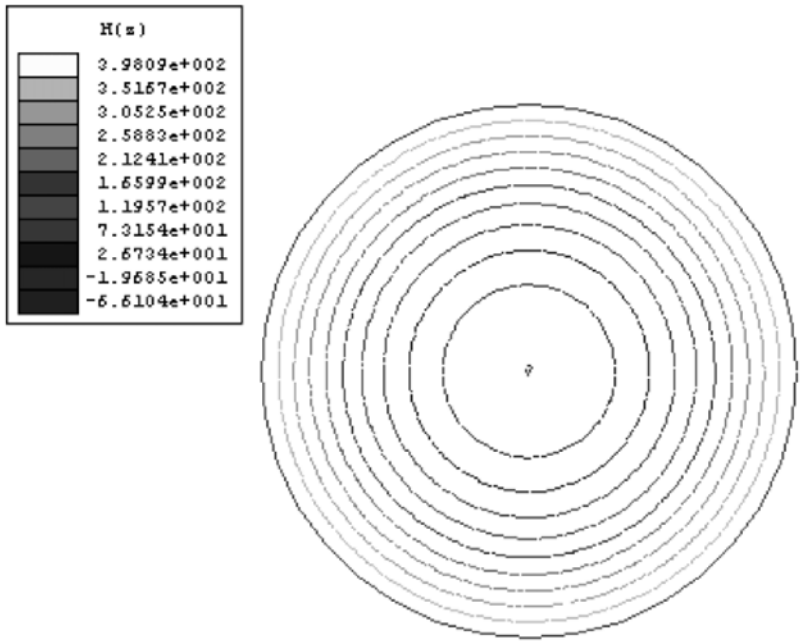

FIGURE 8.5 Computer display of conducting steel cylinder (without cuts) of radius 2.5 mm. The eddy current flow lines are displayed at the instant that the applied outer H of frequency 60 Hz is 398.1 A/m, corresponding to 1 T just inside the outer steel. The contour values show that the real part of H varies from 398.1 down to –66 A/m. The magnetic flux is directed normal to the plane of this figure.

which substituted in (3.8) along with $H = 398.1$ A/m and depth 1 m gives computed DC reluctance $\mathcal{R}_{DC} = 20.26E6$ A/Wb. This value agrees exactly with the value obtained using the conventional magnetostatic reluctance formula (3.9) with area equal to that of the circle.

As mentioned in Chapter 3, AC eddy currents cause reluctance to become complex. The above magnetostatic reluctance $\mathcal{R}_{DC}$ can be compared with the 60 Hz reluctance of Figure 8.5. Using the definition of $\mathcal{R}_{RE}$, the real part of the complex reluctance of (3.16), the software finds $\mathcal{R}_{RE} = 47.57E6$ A/Wb. This is 234.8% of $\mathcal{R}_{DC} = 20.26E6$ A/Wb, and is listed as that percentage in the first row of Table 8.1. As expected from Lenz' law, eddy currents cause the AC reluctance to be higher than the magnetostatic reluctance. Thus the finite-element computations have been verified.

To reduce the AC reluctance and associated eddy power loss, cuts have often been made in solid steel poles and armatures [10]. A similar technique is to use *tape wound* steel, as shown in the spiral steel pole of Figure 8.7. The eddy current flow lines computed by the "Eddy Axial" solver of Maxwell are shown. Note that the circular eddy flow patterns are well blocked by the spiraling. Table 8.1 lists the computed power loss and AC reluctance, both of which are greatly reduced by the spiraling. Thus placing cuts in steel poles can greatly improve their AC performance.

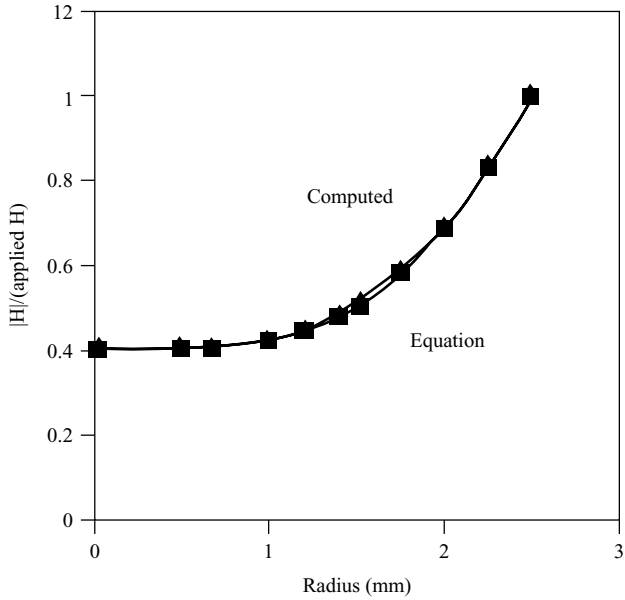

FIGURE 8.6 Ratio of magnitude of H inside steel cylinder over applied H of frequency 60 Hz. The cylinder has a radius of 2.5 mm, a conductivity of 2.E6 S/m, and a relative permeability of 2000. The lower curve is from Equation 8.29, while the upper curve was computed using finite elements.

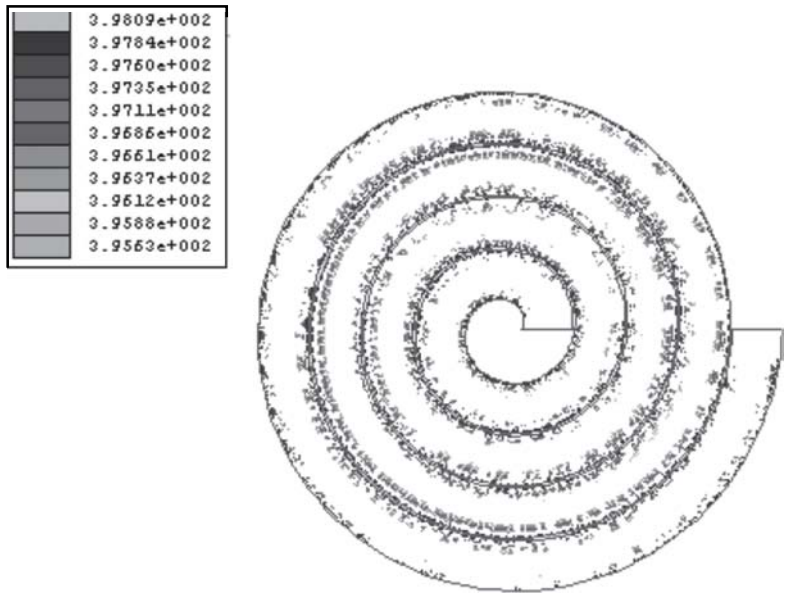

FIGURE 8.7 Computer display of spiral steel pole of radius 2.5 mm and outer $B = 1$ T at 60 Hz, showing computed eddy current flow patterns and contours of constant real H.

TABLE 8.1 Losses and Reluctances Computed for Various (or No) Cuts in Cylinders of Radius 2.5 mm[a]

Cuts	Power Loss (W)	$\mathcal{R}_{RE}/\mathcal{R}_{DC}$ (%)
None	0.481	234.8
Spiral	0.111	100.5
4	0.411	115.7
8	0.198	105.2
36	0.021	111.7

[a]All values are at 60 Hz and with solid steel of conductivity 2.E6 S/m and $B = 1$ T in steel skin.

Example 8.3 Loss and Reluctance of a Cylindrical Pole with Added Radial Slots Figure E8.3.1 shows the cross section of a cylindrical steel pole of radius 2.5 mm. The steel is again assumed to have relative permeability 2000 and conductivity 2.E6 S/m. A 60-Hz magnetic field of 1 T is applied just inside the surface of the cylinder. As shown in Figure E.8.3.1, in an attempt to reduce eddy currents, four radial slots of width 0.03 mm are cut spaced equally. To maintain some mechanical integrity, the slots are only cut down to a radius of 0.55 mm.

Compute the eddy power loss and real AC reluctance $\mathcal{R}_{RE}$ using the finite-element software Maxwell.

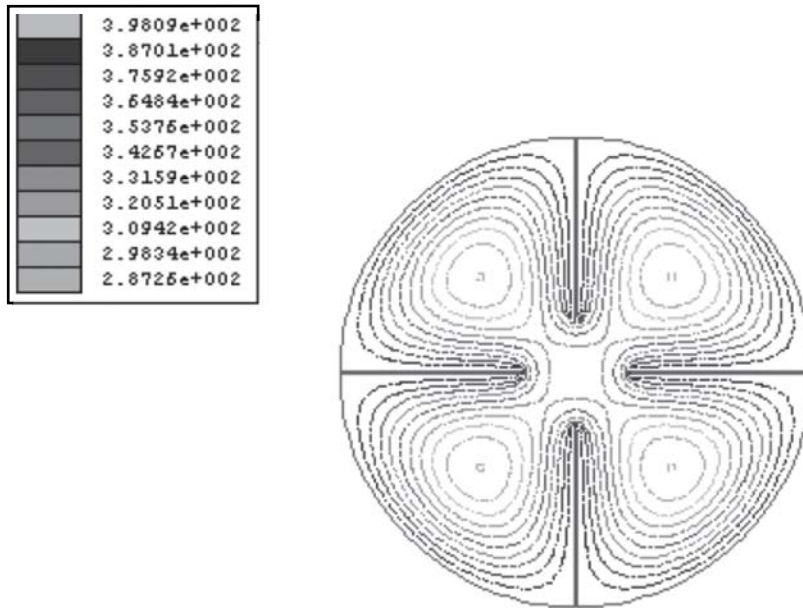

FIGURE E8.3.1 Computer display of steel cylinder with four radial slots and outer $B = 1$ T at 60 Hz, showing computed eddy current flow patterns and contours of constant real H.

Solution Maxwell's "Eddy Axial" is selected as the Solver, along with the default *xy* plane. The applied outer boundary condition is $H_z = 398.1$ A/m to obtain 1 T just inside the steel surface. The resulting plot of contours of real H_z is shown in Figure E8.3.1. The power loss is 0.411 W for 1 m depth and is entered in Table 8.1, where it is seen to be somewhat less than the power loss for no slots. Table 8.1 also lists the computed real AC reluctance as a percentage of the DC reluctance. Note that slotting has significantly reduced the AC reluctance. Table 8.1 also lists computed results with increased numbers of equally spaced slots.

PROBLEMS

8.1 Redo Example 6.5 but at a frequency of 10 Hz.

8.2 Redo Example 6.5 but with a conductivity of 2.E5 S/m.

8.3 Calculate the skin depth at 60 Hz of material with:

(a) A semiconductor with conductivity = 1 S/m and relative permeability = 1.

(b) Copper with conductivity = 5.8E7 S/m and relative permeability = 1.

(c) A high conductivity (5.E6 S/m) steel with relative permeability = 8000.

8.4 Find (in a book containing mathematical series) the complete trigonometric series for (8.11).

8.5 Redo Example 8.1 but with Maxwell's nonlinear "steel_1010."

8.6 Repeat Problem 8.5 but with the current increased to 5 A. Note that Maxwell handles nonlinear *B–H* characteristics in AC eddy current problems, and saturation can affect the equivalent circuit parameters.

8.7 Redo Example 8.2 but with the shading ring moved to an inner radius of 9 mm.

8.8 Redo Example 8.2 but with the shading ring moved to an inner radius of 11 mm.

8.9 Redo Example 8.3 but with eight equally spaced radial slots. Besides obtaining the numerical values in Table 8.1, also obtain a plot of the eddy current flow pattern.

8.10 Redo Example 8.3 but with 36 equally spaced radial slots. Besides obtaining the numerical values in Table 8.1, also obtain a plot of the eddy current flow pattern. Explain why the AC reluctance has not decreased further.

REFERENCES

1. Sadiku M. *Elements of Electromagnetics*, 3rd ed. New York: Oxford University Press; 2001.

2. Brauer JR, Cendes ZJ, Beihoff BC, Phillips KP. Laminated steel eddy current losses versus frequency computed with finite elements. *IEEE Trans Indus Appl* 2000;36:1132–1137.
3. Fitzgerald AE, Kingsley C. *Electric Machinery*, 2nd ed. New York: McGraw-Hill; 1961. pp 346–347.
4. Demerdash NA, Nehl TW. Use of numerical analysis of nonlinear eddy current problems by finite elements in the determination of parameters of electrical machines with solid iron rotors. *IEEE Trans Magn* 1979;15:1482–1484.
5. Juds MA. A nonlinear magnetodynamic model for AC magnets with shading coils, *Proceedings of International Relay Conference*, 1994.
6. Laithwaite ER. *Propulsion without Wheels*, 2nd ed. London: English Universities Press Ltd.; 1970.
7. Laithwaite ER. *Induction Machines for Special Purposes*. New York: Chemical Publishing Co., Inc.; 1966, Chapter 9.
8. Ramo S, Whinnery JR, Van Duzer T. *Fields and Waves in Communication Electronics*. New York: John Wiley & Sons; 1965, pp 292–293.
9. Dwight HB. *Tables of Integrals and other Mathematical Data*. New York: MacMillan Co.; 1961, pp 324–325.
10. Roters HC. *Electromagnetic Devices*. New York: John Wiley & Sons; 1941.